**EPJ manuscript No.**
(will be inserted by the editor)

# Thin-film model of droplet durotaxis

*'E pur si muove'*

Hector Gomez[1,a], Mirian Velay-Lizancos[2]

[1]School of Mechanical Engineering, Purdue University, 585 Purdue Mall, West Lafayette, IN 47907, USA.
[2] Lyles School of Civil Engineering, Purdue University, 550 W Stadium Ave, West Lafayette, IN 47907, USA.

**Abstract.** The control of liquid droplets on solid surfaces is important in many scientific and technological applications, including microfabrication, microfluidics and heat transfer. It has been known for decades that droplets sitting on a solid surface can be moved using thermal, chemical or electrical gradients. Recent experiments have shown that gradients of substrate deformability also produce spontaneous droplet motion. This motion mechanism, which is called durotaxis, remains poorly understood. This paper proposes a model for droplet durotaxis based on a thin-film description of the fluid dynamics equation. The substrate is modeled as a Kirchhoff plate with non-constant flexural rigidity. We use high-fidelity simulations to show that the model naturally predicts droplet durotaxis without any *ad hoc* assumption. The model predictions for the dependence of droplet velocity on droplet size are consistent with experiments. The simplicity of the model suggests that durotaxis may be a pervasive and fundamental process at small scales and opens new possibilities to study the interaction of droplets with compliant solid surfaces.

## 1 Introduction

The controlled motion of liquid droplets on solid substrates plays a key role in, e.g., microfabrication [10,33,23,32], microfluidics [11,22,8,37] and surface coatings [6,28, 36] and is an ubiquitous example of mass transport by propagation of phase interfaces. Classical mechanisms for producing droplet motion consist of generating, e.g., a temperature gradient [2] or a wettability gradient induced by a chemical compound [24,6]. Recent experiments found a different type of free-running droplets in which the motion is produced by a gradient in the substrate strains [3] or stiffness [31]. The motion of droplets driven by stiffness gradients is referred to as *durotaxis* and is relevant at small scales, where the gas-liquid surface tension and the overpressure in the droplet (also known as Laplace pressure) are strong enough to significantly deform the substrate. Standard scaling arguments can be used to show that this occurs for droplets with radius comparable to the elastocapillary length scale, i.e.,

[a] e-mail: `hectorgomez@purdue.edu`

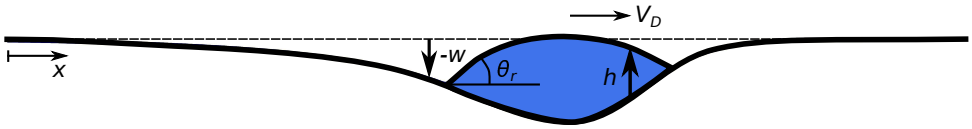


**Fig. 1.** One-dimensional representation of the studied system. The plate deflection $w$ is negative when the deformed configuration is below the undeformed one. The thin-film thickness $h$ is measured from the deformed configuration of the substrate. The angle $\theta_r$ represents the receding apparent contact angle and $V_D$ is the droplet velocity.

$l_{EC} = \sqrt{\gamma/E}$, where $\gamma$ is the surface tension at the liquid-gas interface and $E$ is the substrate Young's modulus [30].

Droplet durotaxis has drawn significant attention, leading to multiple experimental [31,19] and computational studies [4]. Droplet durotaxis is currently explained using the concept of apparent contact angle, i.e., the angle of the liquid-gas interface at the contact line *relative to the undeformed solid surface*. It was proposed that the droplet moves in the direction of lower apparent contact angle similarly to the motion driven by a wettability gradient. This mechanism was consistent with the full-scale three-dimensional simulations presented in [4]. The computational results shown in [4] resolve in a fully-coupled manner the velocity and pressure fields in the gas and the liquid as well as the solid displacements using a fully nonlinear formulation. The simulations show that although the droplet always moves in the direction of lower apparent contact angle, the motion can be inverted by changing the fluid's wettability — while wetting droplets move toward softer areas of the substrate, non-wetting droplets advance in the direction in which stiffness increases.

Here, we propose a simplified model of droplet durotaxis based on the asymptotic reduction of the fluid and solid dynamics equations. The model predicts durotaxis and preserves all the key features of the process, including the dependence of the droplet velocity on its size and the motion in the direction of the lower apparent contact angle. The proposed model relies on a description of the fluid dynamics based on the thin-film approximation and a linear Kirchhoff plate model. Our results suggest that the process of durotaxis does not depend on the details of the three-dimensional solid deformation, including the ridge at the contact line, but only on the global deformation of the substrate. The proposed simplified model allows fast simulations and systematic parametric studies which may shed light on the intriguing process of droplet durotaxis.

## 2 Thin-film model of droplet durotaxis

The study of a liquid layer on a smooth solid surface has been traditionally studied under the assumption of a rigid solid. A notable exception can in found in [38]. This paper considers a deformable membrane but neglects surface tension effects, which are crucial for droplet durotaxis. Under the so-called long wave approximation [21] and under the assumption of small Bond numbers, the Navier-Stokes equations can be simplified to an evolution equation for the thin-film thickness profile $h$; see a one-dimensional representation in Fig. 1. When the substrate is compliant and is subjected to a vertical displacement $w$, we propose that the thin-film equation is given by

$$\frac{\partial h}{\partial t} + \nabla \cdot \left( \frac{h^3}{3\eta} \nabla \Big( \Pi(h) + \gamma \Delta (h + w) \Big) \right) = 0 \tag{1}$$

where $\eta$ is the fluid dynamic viscosity, $\gamma$ is the surface tension at the liquid-gas interface and $\Pi(h)$ is the so-called disjoining pressure that accounts for the wetting

properties of the substrate [17]. Note that $h$ represents the thickness of the fluid measured from the deformed configuration of the substrate. By taking $w = 0$ in Eq. (1), a classical thin-film model is retrieved. Energetic arguments may be used to prove that the last term in Eq. (1) is the leading-order approximation to the surface tension contribution when the substrate is deformable.

Although not widely used, the classical plate theory was developed for plates with non-constant flexural rigidity. Given that the load produced by the droplet on the plate is $\Pi(h)+\gamma\Delta(h+w)$, the force balance equation on the plate may be written as

$$\Delta(D\Delta w) - (1-\nu)\diamondsuit^2(D,w) = \Pi(h) + \gamma\Delta(h+w) \tag{2}$$

where $\diamondsuit^2(D,w) = \Delta D\Delta w - \nabla\nabla D : \nabla\nabla w$, $\nu$ is the solid's Poisson ratio and $D(\boldsymbol{x})$ is the flexural rigidity which can be written as $D = E\epsilon^3/[12(1-\nu^2)]$. Here, $E$ is the Young's modulus and $\epsilon$ is the plate thickness.

To complete the model definition, we need an expression for the disjoining pressure. We use the function [27]

$$\Pi(h) = 2S_a d_0^2/h^3 + (S_p/\ell)\exp[(d_0-h)/\ell] \tag{3}$$

where $d_0 = 0.158$ nm is the Born repulsion length and $\ell$ is the correlation length of a polar fluid. For water, $\ell \approx 0.6$ nm [35]. The parameters $S_a$ and $S_p$ are, respectively, the apolar and polar components of the total spreading coefficient $S = S_a + S_p$. We take $S_a > 0$ and $S_p < 0$, which represents a destabilizing short-range polar interaction combined with a stabilizing long-range apolar van der Waals force. Experimental systems corresponding to this case are, e.g., water on graphite [34] and on most polar substrates like Poly(methyl methacrylate) (PMMA), PVC or polystyrene [26]. For this parameter regime, Eq. (1) admits solutions representing a static droplet with an equilibrium contact angle $\theta_e = \arccos(S/\gamma+1)$ sitting on an ultrathin precursor film.

Because the flexural rigidity $D$ is a function of space, let us introduce the notation $D(\boldsymbol{x}) = D_0 R(\boldsymbol{x})$, where $D_0$ is a flexural rigidity scale and $R(\boldsymbol{x})$ is a dimensionless function of space. By scaling space with $\ell$ and time with $3\eta\ell|S_p|^{-1}e^{-d_0/\ell}$, the governing equations can be written in dimensionless form as

$$\frac{\partial h}{\partial t} + \nabla\cdot\Big(h^3\nabla\Big(M_i/h^3 - e^{-h} + S_c\Delta(h+w)\Big)\Big) = 0 \tag{4}$$

$$\Sigma^{-1}\Delta(R\Delta w) - \Sigma^{-1}(1-\nu)\diamondsuit^2(R,w) = M_i/h^3 - e^{-h} + S_c\Delta(h+w) \tag{5}$$

where we have introduced the following dimensionless numbers

$$M_i = 2\frac{S_a}{|S_p|}\left(\frac{d_0}{\ell}\right)^2 e^{-d_0/\ell}, \quad S_c = \frac{\gamma}{|S_p|}e^{-d_0/\ell}, \quad \Sigma = \frac{|S_p|\ell^2}{D_0}e^{d_0/\ell}. \tag{6}$$

Note that although we have kept the original notation for $h$ and $w$ for simplicity, the functions in Eqns. (4)–(5) have been non-dimensionalized using the above-defined length and time scales. From now on, we will always work with the dimensionless form of the equations.

## 3 Computational method

Solving numerically Eqns. (4)–(5) is challenging for multiple reasons, including (a) the difficulty of discretizing fourth-order spatial derivatives, (b) the challenge of solving in a coupled manner an evolution equation for $h$ and an equation that operates at an

infinitely fast time scale for $w$, (c) the singular behavior of the disjoining pressure as $h \to 0$, which requires an extremely accurate solution to Eq. (5) each time step.

For the space discretization, we propose an algorithm based on isogeometric analysis, a recent generalization of the finite element method that uses as basis functions splines of controllable continuity across the element boundaries [16,9]. The use of isogeometric analysis permits a straightforward discretization of the fourth-order derivatives in Eqns. (4)–(5). Our algorithm is based on the following weak form of the equations, which may be derived multiplying them with smooth weight functions $p$ and $q$, integrating over the computational domain $\Omega$ and applying the divergence theorem multiple times. Assuming natural boundary conditions for the fluid dynamics equation and considering a clamped plate, our weak form can be written as

$$\int_\Omega p\frac{\partial h}{\partial t}\mathrm{d}x - \int_\Omega h^3\nabla p\cdot\nabla\left(M_i/h^3 - e^{-h}\right)\mathrm{d}x + \int_\Omega \nabla\cdot\left(h^3\nabla p\right)S_c\Delta(h+w)\mathrm{d}x = 0, \quad (7)$$

$$\int_\Omega \Delta q\frac{R}{\Sigma}\Delta w\mathrm{d}x - \int_\Omega q\left(\frac{1-\nu}{\Sigma}\diamondsuit^2(R,w) + M_i/h^3 - e^{-h}\right)\mathrm{d}x + \int_\Omega S_c\nabla q\cdot\nabla(h+w)\mathrm{d}x = 0, \quad (8)$$

These equations must be satisfied for all $p$ and $q$ in suitable functional spaces. The discretization of the weak form can be accomplished by defining finite dimensional spline spaces [16,12] that are used to construct approximations to the unknowns $h$ and $w$ as well as to the weight functions [14,15].

The time discretization is performed using a staggering scheme. By choosing a sufficiently small time step $\Delta t$, we compute the approximate solution at time $t_{n+1} = t_n + \Delta t$ by $(i)$ obtaining an approximate solution to $h(\cdot, t_{n+1})$ time discretizing Eq. (7) by the generalized-$\alpha$ method [7,18], $(ii)$ using the approximation to $h(\cdot, t_{n+1})$ in Eq. (8) to obtain an approximation to $w(\cdot, t_{n+1})$, and $(iii)$ utilizing the most current value of $w(\cdot, t_{n+1})$ to obtain an updated approximation to $h(\cdot, t_{n+1})$ by solving again Eq. (7). We observed that additional iterations between Eqns. (7) and (8) within a time step increased the compute time without showing significant stability or accuracy improvements. We have found that the proposed staggering scheme was more effective than solving monolithically Eqns. (7)-(8). The resulting algebraic equations were linearized using the Newton-Raphson algorithm and the linear systems of equations were solved using diagonally preconditioned GMRES [25].

As noted above the interstitial pressure $\Pi(h) = M_i/h^3 - e^{-h}$ is singular at $h = 0$. This implies that an inaccurate solution to Eq. (8), can produce a very large load on the plate in the next time step. Although all the simulations presented in this paper are overkilled solutions to Eqns. (7)–(8) considering all terms, we have observed that neglecting the term $M_i/h^3 - e^{-h}$ in Eq. (8) produces qualitatively similar solutions at a much smaller computational cost.

## 4 Results

We study the proposed model by performing one-dimensional simulations on the computational domain $\Omega = [0, L]$ with $L = 1000$. In the simulations presented in this paper, we used 512 uniform elements in space and a time step $\Delta t = 50$. The function $R(x)$, which defines the spatial variation of the flexural rigidity, is given by $R(x) = e^{-Gx}$, where $G$ is a dimensionless parameter. We took $G = 7 \cdot 10^{-3}$ in all of our calculations. We begin our simulations by placing a droplet at the center of the domain on top of an ultrathin film. Our initial condition is given by

$$h(x,0) = h_{ut} + \max\left(0, h_{\max}\left[1 - \left(\frac{x - L/2}{R}\right)^2\right]\right) \quad (9)$$

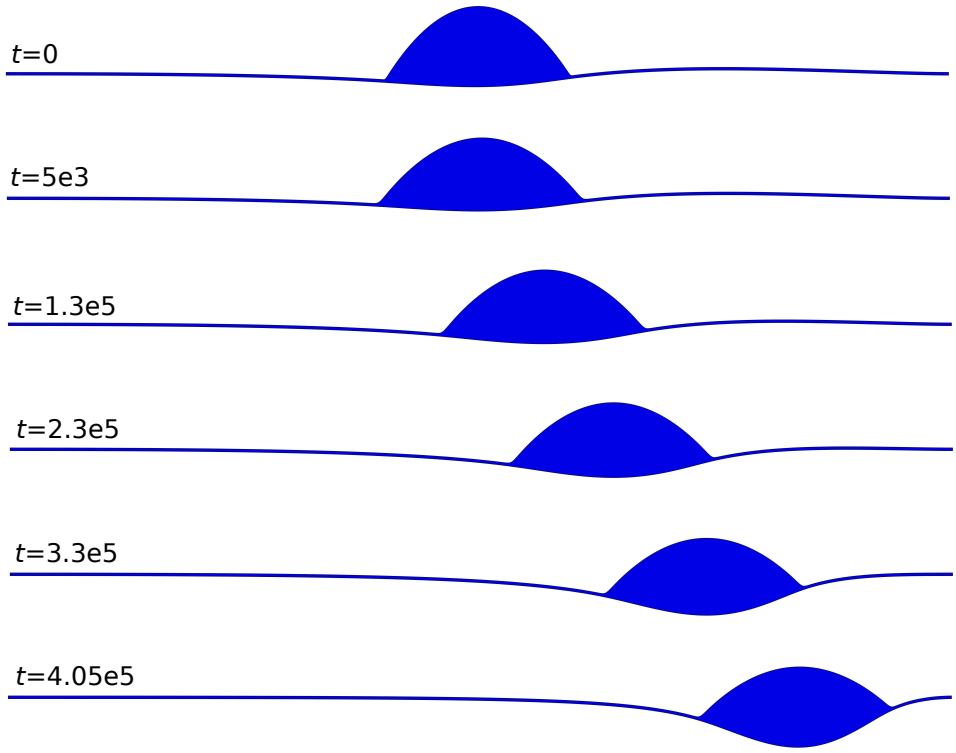


**Fig. 2.** Time evolution of a droplet on a compliant Kirchhoff plate with non-constant flexural rigidity. The values of the non-dimensional groups are $M_i = 0.5$, $S_c = 1$, $\Sigma = 10^{-6}$, $G = 7 \cdot 10^{-3}$. The system size is $L = 1000$. The mesh is composed of 512 uniform elements and the time step is $\Delta t = 50$. Snapshots of the droplet evolution on the deformed plate.

where $h_{ut} = 1.1738$ represents the thickness of the precursor film, $2R$ is the size of the wetted area under the droplet and $h_{ut} + h_{\max} \approx h_{\max}$ is the maximum film thickness achieved at the centerline of the droplet. For this initial condition, the volume (area in our one-dimensional simulation) of the droplet is approximately $V = 4h_{\max}R/3$ and the initial contact angle is $\theta_0 = \arctan(2h_{\max}/R)$. In our simulations, we varied $h_{\max}$ and $R$, but always kept constant the ratio $h_{\max}/R$ which resulted in $\theta_0 \approx 32.62°$

Fig. 2 shows the time evolution of a droplet with $h_{\max} = 420/13$ and $R = 100$. The thin blue stripes on the left and right hand sides of the droplet represent the precursor film that sits right on top of the Kirchhoff plate (not shown for clarity). The configuration at time $t = 0$ was obtained by solving Eq. (8) with the given initial condition $h(x, 0)$. The Laplace pressure under the droplet and the surface tension at the contact line produce a deformation of the plate. It is apparent from the simulation that the droplet moves spontaneously to the right-hand side, the softer area of the substrate. The result is consistent with experiments [31] and with the full-scale three-dimensional simulations of wetting droplets presented in [4]. It may be observed that the droplet accelerates throughout the process and sinks deeper into the substrate as time evolves. It is remarkable that such a simple model can predict durotaxis because the solid model is very elementary, and in particular, misses completely the ridge that is usually formed under the contact line; see [5, 4, 1, 29, 20]. Fig. 3 shows the time

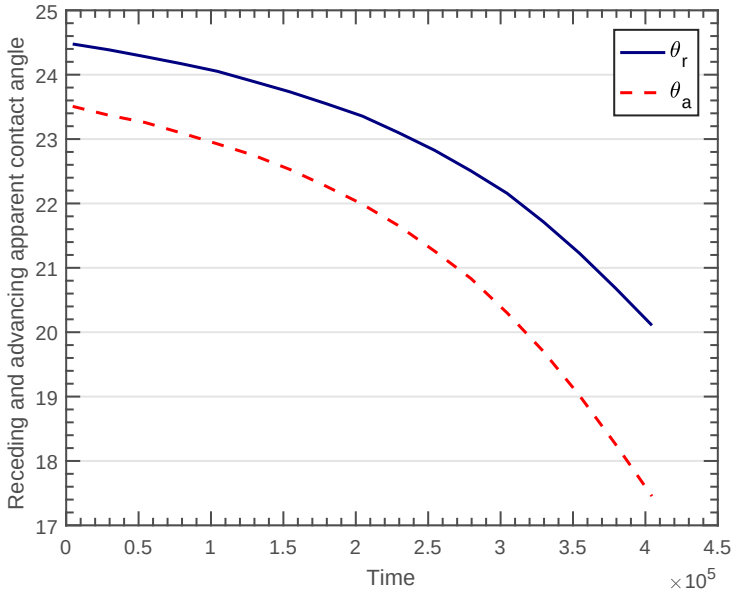


**Fig. 3.** Time evolution of the receding and advancing apparent contact angles for the simulation shown in Fig. 2. We observe that the advancing contact angle is lower than the receding contact angle.

evolution of the receding and advancing *apparent* contact angles. We observe that the advancing angle is lower than the receding angle, which is compatible with the mechanism for durotactic droplet motion proposed in [31].

Fig. 4 shows the time evolution of the droplet centerline for three droplets of different sizes. The droplet centerline was defined as the midpoint between the left and right contact lines. The droplet size is defined by the parameter $R$; cf. with Eq. (9). The dimensionless parameters are identical to those used in the simulation shown in Fig. 2. Consistently with the experiments in [31], larger droplets move faster, presumably because the stiffness difference between the left and right triple points is larger.

To further study droplet durotaxis, we tested the relation $V_D = kS_c\Delta\theta$, where $V_D$ is the dimensionless droplet velocity and $k$ is a fitting constant. This relation follows from dimensional analysis under the assumption that $\Delta\theta$ is small. In particular, the expression shows that data for droplets of different sizes should collapse on the same curve. We used our simulations to test this relation. Direct numerical differentiation of the data for the droplet position over time produced large oscillations because the displacement data is not smooth; see inset in Fig. 4. The roughness of the displacement data may be attributed to inaccuracies in the identification of the contact lines or stick-slip behavior. To bypass this obstacle, we interpolated the displacement data with a cubic polynomial, which resulted in a very accurate approximation. Then, we we computed the velocity differentiating the polynomial. Fig. 5 shows the comparison of the theoretical relation $V_D = kS_c\Delta\theta$ and the numerical results. The agreement is good, especially for small $\Delta\theta$.

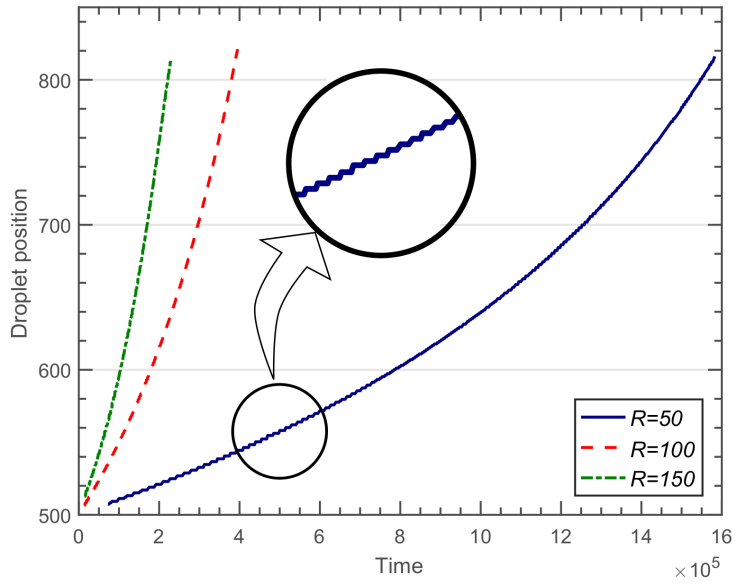


**Fig. 4.** Dependence of the droplet velocity on its size. The values of the non-dimensional groups are $M_i = 0.5$, $S_c = 1$, $\Sigma = 10^{-6}$, $G = 7 \cdot 10^{-3}$. The system size is $L = 1000$. The mesh is composed of 512 uniform elements and the time step is $\Delta t = 50$. Time evolution of the droplet centerline for droplets of different sizes.

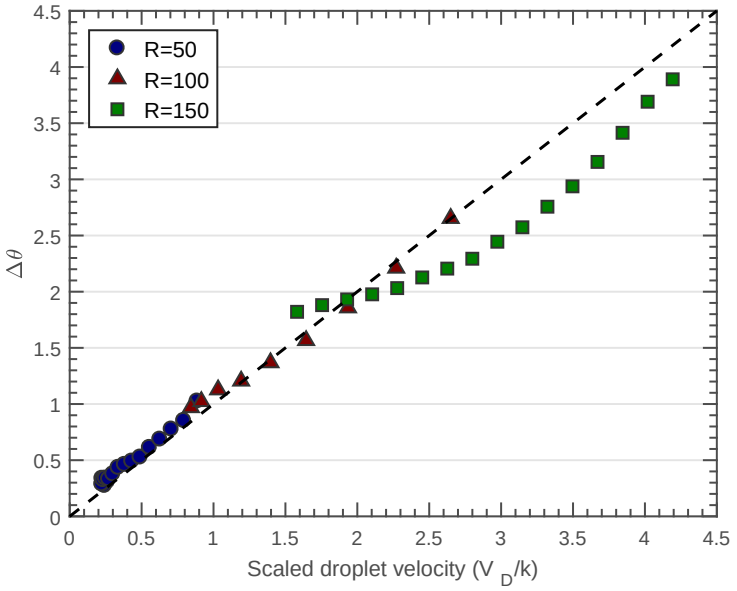


**Fig. 5.** Comparison of the theoretical relation $V_D = kS_c\Delta\theta$ that follows from dimensional analysis under the assumption of small $\Delta\theta$ (dashed black line) with the results of our numerical simulations for $R = 50$ (circles), $R = 100$ (triangles), and $R = 150$ (squares). The data corresponds to the simulations shown in Fig. 4.

## 5 Conclusions

The control of individual droplets on solid surfaces is at the core of many technological applications, including digital microfluidics, heat transfer and self-cleaning surfaces. The use of solid substrates with spatial gradients of stiffness is a recently proposed mechanism for spontaneous droplet motion called durotaxis. Here, we have shown that droplet durotaxis can be explained with a surprisingly simple model that couples a thin-film description of the fluid dynamics equations and a Kirchhoff plate model for the solid substrate. Direct numerical simulation of the proposed model shows compatible results with experiments in terms of dependence of droplet velocity on droplet size. The simulations also suggest that droplet motion can be explained by a difference in apparent contact angle at each side of the droplet. Our simple model opens new possibilities to interrogate interactions between droplets and compliant substrates [5, 13].

## References

1. José Bico, Étienne Reyssat, and Benoît Roman. Elastocapillarity: When surface tension deforms elastic solids. *Annual Review of Fluid Mechanics*, 50:629–659, 2018.
2. Françoise Brochard. Motions of droplets on solid surfaces induced by chemical or thermal gradients. *langmuir*, 5(2):432–438, 1989.
3. Jesus Bueno, Yuri Bazilevs, Ruben Juanes, and Hector Gomez. Droplet motion driven by tensotaxis. *Extreme Mechanics Letters*, 13:10–16, 2017.
4. Jesus Bueno, Yuri Bazilevs, Ruben Juanes, and Hector Gomez. Wettability control of droplet durotaxis. *Soft matter*, 14(8):1417–1426, 2018.
5. Jesus Bueno, Hugo Casquero, Yuri Bazilevs, and Hector Gomez. Three-dimensional dynamic simulation of elastocapillarity. *Meccanica*, 53(6):1221–1237, 2018.
6. Manoj K Chaudhury and George M Whitesides. How to make water run uphill. *Science*, 256(5063):1539–1541, 1992.
7. J. Chung and G.M. Hulbert. A time integration algorithm for structural dynamics with improved numerical dissipation: The generalized-$\alpha$ method. *Journal of Applied Mechanics*, 60:371–375, 1993.
8. N. J. Cira, A. Benusiglio, and M. Prakash. Vapour-mediated sensing and motility in two-component droplets. *Nature*, 519(7544):446–450, 2015.
9. J.A. Cottrell, T.J.R. Hughes, and Y. Bazilevs. *Isogeometric Analysis: Toward Integration of CAD and FEA*. Wiley, 2009.
10. Michaël De Volder and A John Hart. Engineering hierarchical nanostructures by elastocapillary self-assembly. *Angewandte Chemie International Edition*, 52(9):2412–2425, 2013.
11. Paul Drzaic. Displays: Microfluidic electronic paper. *Nature Photonics*, 3(5):248–249, 2009.
12. H. Gomez, V.M. Calo, Y. Bazilevs, and T.J.R. Hughes. Isogeometric analysis of the cahn–hilliard phase-field model. *Computer methods in applied mechanics and engineering*, 197(49):4333–4352, 2008.
13. Hector Gomez and Jesus Bueno. Interaction of multiphase fluids and solid structures. In *Frontiers in Computational Fluid-Structure Interaction and Flow Simulation*, pages 131–165. Springer, 2018.
14. Hector Gomez, Thomas JR Hughes, Xesús Nogueira, and Victor M Calo. Isogeometric analysis of the isothermal navier–stokes–korteweg equations. *Computer Methods in Applied Mechanics and Engineering*, 199(25-28):1828–1840, 2010.
15. Hector Gomez and Kristoffer G van der Zee. Computational phase-field modeling. *Encyclopedia of Computational Mechanics Second Edition*, pages 1–35, 2018.
16. Thomas JR Hughes, John A Cottrell, and Yuri Bazilevs. Isogeometric analysis: Cad, finite elements, nurbs, exact geometry and mesh refinement. *Computer methods in applied mechanics and engineering*, 194(39-41):4135–4195, 2005.

17. Jacob N Israelachvili. *Intermolecular and surface forces*. Academic press, 2011.
18. K.E. Jansen, C.H. Whiting, and G.M. Hulbert. A generalized-$\alpha$ method for integrating the filtered Navier-Stokes equations with a stabilized Finite Element Method. *Computer Methods in Applied Mechanics and Engineering*, 190(34):305 – 319, 2000.
19. Tianshu Liu, Nichole Nadermann, Zhenping He, Steven H Strogatz, Chung-Yuen Hui, and Anand Jagota. Spontaneous droplet motion on a periodically compliant substrate. *Langmuir*, 33(20):4942–4947, 2017.
20. Robin Masurel, Matthieu Roché, Laurent Limat, Ioan Ionescu, and Julien Dervaux. Elastocapillary ridge as a noninteger disclination. *Physical Review Letters*, 122(24):248004, 2019.
21. Alexander Oron, Stephen H Davis, and S George Bankoff. Long-scale evolution of thin liquid films. *Reviews of modern physics*, 69(3):931, 1997.
22. M. Prakash and N. Gershenfeld. Microfluidic bubble logic. *Science*, 315(5813):832–835, 2007.
23. O. Raccurt, F. Tardif, F. A. d'Avitaya, and T. Vareine. Influence of liquid surface tension on stiction of SOI MEMS. *Journal of Micromechanics and Microengineering*, 14(7):1083, 2004.
24. E Raphaël. Cr acad. sci., ser. *IIb*, 306:751, 1988.
25. Y. Saad and M.H. Schultz. GMRES: A generalized minimal residual algorithm for solving nonsymmetric linear systems. *SIAM Journal on Scientific and Statistical Computing*, 7(3):856–869, July 1986.
26. Ashutosh Sharma. Equilibrium contact angles and film thicknesses in the apolar and polar systems: Role of intermolecular interactions in coexistence of drops with thin films. *Langmuir*, 9(12):3580–3586, 1993.
27. Ashutosh Sharma. Relationship of thin film stability and morphology to macroscopic parameters of wetting in the apolar and polar systems. *Langmuir*, 9(3):861–869, 1993.
28. Mordechai Sokuler, Gunter K Auernhammer, Marcel Roth, Chuanjun Liu, Elmar Bonacurrso, and Hans-Jurgen Butt. The softer the better: fast condensation on soft surfaces. *Langmuir*, 26(3):1544–1547, 2009.
29. Robert W Style, Rostislav Boltyanskiy, Yonglu Che, JS Wettlaufer, Larry A Wilen, and Eric R Dufresne. Universal deformation of soft substrates near a contact line and the direct measurement of solid surface stresses. *Physical review letters*, 110(6):066103, 2013.
30. Robert W Style, Anand Jagota, Chung-Yuen Hui, and Eric R Dufresne. Elastocapillarity: Surface tension and the mechanics of soft solids. *Annual Review of Condensed Matter Physics*, 8:99–118, 2017.
31. R.W. Style, Y. Che, S.J. Park, B.M. Weon, J.H. Je, C. Hyland, G.K. German, M.P. Power, L.A. Wilen, J.S. Wettlaufer, et al. Patterning droplets with durotaxis. *Proceedings of the National Academy of Sciences*, 110(31):12541–12544, 2013.
32. T. Tanaka, M. Morigami, and N. Atoda. Mechanism of resist pattern collapse during development process. *Japanese Journal of Applied Physics*, 32(12S):6059, 1993.
33. S. H. Tawfick, J. Bico, and S. Barcelo. Three-dimensional lithography by elasto-capillary engineering of filamentary materials. *MRS Bulletin*, 41(02):108–114, 2016.
34. Uwe Thiele, Michael Mertig, and Wolfgang Pompe. Dewetting of an evaporating thin liquid film: Heterogeneous nucleation and surface instability. *Physical review letters*, 80(13):2869, 1998.
35. CJ Van Oss. Surface free energy contribution to cell interactions. In *Biophysics of the Cell Surface*, pages 131–152. Springer, 1990.
36. Tak-Sing Wong, Sung Hoon Kang, Sindy KY Tang, Elizabeth J Smythe, Benjamin D Hatton, Alison Grinthal, and Joanna Aizenberg. Bioinspired self-repairing slippery surfaces with pressure-stable omniphobicity. *Nature*, 477(7365):443, 2011.
37. Benzhong Zhao, Christopher W. MacMinn, and Ruben Juanes. Wettability control on multiphase flow in patterned microfluidics. *Proceedings of the National Academy of Sciences*, 113(37):10251–10256, 2016.
38. Zhong Zheng, Ian M Griffiths, and Howard A Stone. Propagation of a viscous thin film over an elastic membrane. *Journal of Fluid Mechanics*, 784:443–464, 2015.